ACS APPLIED MATERIALS & INTERFACES

Research Article

www.acsami.org

# Uniform, Homogenous Coatings of Carbon Nanohorns on Arbitrary Substrates from Common Solvents

Landon Oakes,[†,‡] Andrew Westover,[†,‡] Masoud Mahjouri-Samani,[§] Shahana Chatterjee,[†] Alexander A. Puretzky,[§] Christopher Rouleau,[§] David B. Geohegan,[§] and Cary L. Pint*[,†,‡]

[†]Department of Mechanical Engineering and [‡]Interdisciplinary Materials Science Program, Vanderbilt University, Nashville, Tennessee, United States

[§]Center for Nanophase Materials Sciences and Materials Science Division, Oak Ridge National Laboratory, Oak Ridge, Tennessee, United States

Supporting Information

**ABSTRACT:** We demonstrate a facile technique to electrophoretically deposit homogenous assemblies of single-walled carbon nanohorns (CNHs) from common solvents such as acetone and water onto nearly any substrate including insulators, dielectrics, and three-dimensional metal foams, in many cases without the aid of surfactants. This enables the generation of pristine film-coatings formed on time scales as short as a few seconds and on three-dimensional templates that enable the formation of freestanding polymer-CNH supported materials. As electrophoretic deposition is usually only practical on conductive electrodes, we emphasize our observation of efficient deposition on nearly any material, including nonconductive substrates. The one-step versatility of deposition on these materials provides the capability to directly assemble CNH materials onto functional surfaces for a broad range of applications. In this manner, we utilized as-deposited CNH films as conductometric gas sensors exhibiting better sensitivity in comparison to equivalent single-walled carbon nanotube sensors. This gives a route toward scalable and inexpensive solution-based processing routes to manufacture functional nanocarbon materials for catalysis, energy, and sensing applications, among others.

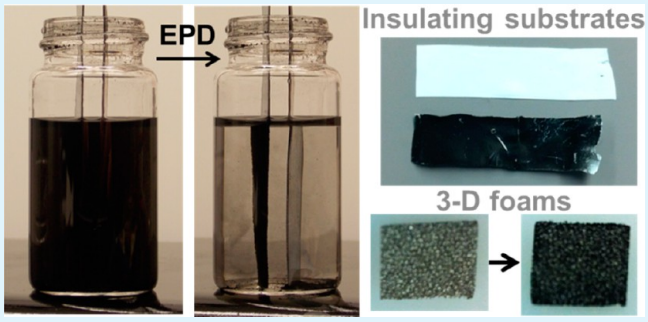


**KEYWORDS:** *carbon nanohorns, electrophoretic deposition, gas sensing, coatings, three-dimensional foams*

## INTRODUCTION

The integration of carbon nanomaterials into functional applications depends on the ability to either grow the materials in functional templates, or assemble them from bulk nanomaterials posthumously. This has led to a significant amount of efforts focused on the growth of carbon nanotubes (CNTs) and graphene in functional three-dimensional architectures that are viable for a broad range of applications.[1−5] Alternatively, materials such as fibers and films have been developed using liquid processing techniques that require homogenous dispersions of nanocarbons in liquids.[6−12] Assembly into homogenous two- and three-dimensional materials can then take place either by utilizing extrusion of the dispersion into fibers, filtration, or electrokinetic manipulation in some cases.[6,8,13] Whereas the majority of such studies have focused on CNT and graphene materials, carbon nanohorns (CNHs) and particularly single-walled CNHs are also a promising nanostructure that offers complementary properties to other forms of nanocarbons.[14−16] CNHs exhibit a high-surface-area architecture that, unlike CNTs and graphene, hosts a large number of reactive $sp^3$ carbon edge sites that makes them ideal for sensing,[14] energy storage,[17,18] or catalytic applications.[19] However, because it is not currently possible to directly grow CNHs in self-assembled architectures, liquid-based processing and manufacturing routes must be developed to enable CNH materials that can be viable for applications. From a production standpoint, these materials can be produced in large quantities (kg/day) with substantial control over their morphological features.[20−22] Despite these advancements, nearly all applications for these materials require controlled assembly of CNH nanostructures into macroscopic materials, which we demonstrate here to be efficiently accomplished through electrophoretic deposition (EPD).

In recent years, numerous reports have discussed EPD of CNTs and graphene materials to enable the development of a broad range of applications.[1,23−26] EPD is a process that operates based on an electric field generated between two electrodes in solution that causes nanostructures having charged surface sites to exhibit mobility toward the electrode with an opposing charge.[27,28] The surface charge in the case of

Received: September 25, 2013
Accepted: December 2, 2013
Published: December 2, 2013

  

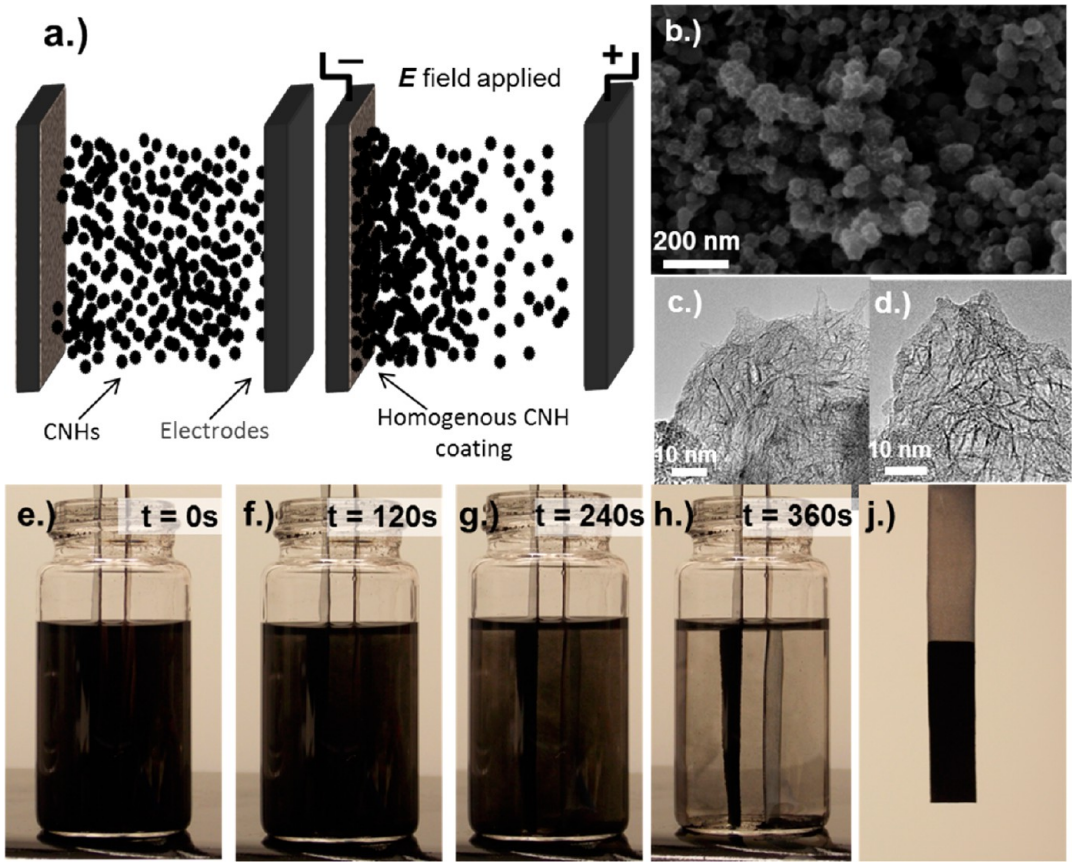


**Figure 1.** (a) Schematic of electrophoretic deposition of carbon nanohorns showing the formation of a homogenous film under an applied electric field. (b) SEM image of a CNH assembly, (c, d) TEM images of representative CNHs studied in this work, and (e−h) photos of a time series of CNH deposition starting from a 0.5 mg/mL CNH/acetone solution after application of a 4 kV/m electric field, showing the complete deposition of CNHs onto the electrode. (j) Photograph of the electrode coated through steps e−h, emphasizing the thick, uniform coating that is studied in this work.

carbon nanomaterials can be either due to the presence of surface functional groups, such as OH− groups, or through the charged groups in surfactants that are applied to carbon nanomaterials to enable dispersion. Following the diffusion of the nanomaterial to the electrode surface, deposition takes place through a mechanism that remains poorly understood.[27] For pristine graphene and CNTs in particular, their poor miscibility in solvents requires the use of surfactants to form stable suspensions except in the unique cases of a few highly polar solvents or superacids.[7,10,11,29−31] However, because of the edge $sp^3$ carbon sites in CNHs, they exhibit much more versatile miscibility in solvents even though no reports have documented the use of EPD as a viable technique to deposit CNH materials. Furthermore, EPD is typically considered a viable tool for deposition onto conductive structures, and whereas there have been a few reports of EPD onto nonconductive surfaces, this generally remains poorly understood and unstudied in the case of carbon nanomaterials.[32−35]

In this study, we document EPD of single-walled CNHs from a variety of common solvents (acetone, tetrahydrofuran (THF), and water) chosen due to their potential for scalability and inexpensive process design. We further emphasize the versatility of this technique by showing the deposition of CNHs directly onto non-conductive surfaces, in addition to three-dimensional (3D) conductive substrates capable of serving as templates to yield free-standing structures of CNHs and CNH-polymer materials. On the basis of the versatile deposition process observed, we describe the mechanism of deposition based on flocculation that occurs near the electrode-solvent interface driven by strong CNH−CNH van der Waals interactions. Furthermore, we utilize this technique for a one-step fabrication of film-based conductometric sensors with higher sensitivity in comparison to equivalent single-walled CNT films. This emphasizes a route toward the nanomanufacturing of functional carbon-based materials where CNHs could play an active role in catalysis, energy storage, sensing, and other application templates.

## EXPERIMENTAL SECTION

**2.1. Single-Walled CNH Synthesis.** Single-walled CNHs were synthesized using high power laser vaporization.[16,36−38] A quartz tube (7.6 cm diameter, 122 cm length) is mounted inside a hinged tube furnace operating up to 1150 °C. The ends of the quartz tube were O-ring sealed with vacuum flanges and the entire system evacuated by a mechanical pump to control the growth environment. Argon is introduced around the laser entrance window to maintain specified pressures and flow rates to carry CNHs out of the furnace into a collection chamber fitted with a HEPA filter. The Nd:YAG laser light (wavelength 1.064 $\mu$m) is delivered through a 0.6 mm diameter fiber optic cable and focused through an anti-reflection coated window onto a target positioned in the center of furnace. CNHs are produced at the optimized laser parameters using 20 ms laser pulses, 90 J/pulse at low laser pulse repetition rate of 5 Hz. The collimating ($f$ = 20 cm) and focusing ($f$ = 1 m) lenses mounted on a robotic arm can be moved to scan the laser beam (4 mm spot diameter) across the target in pre-designed raster patterns to achieve uniform target erosion during long

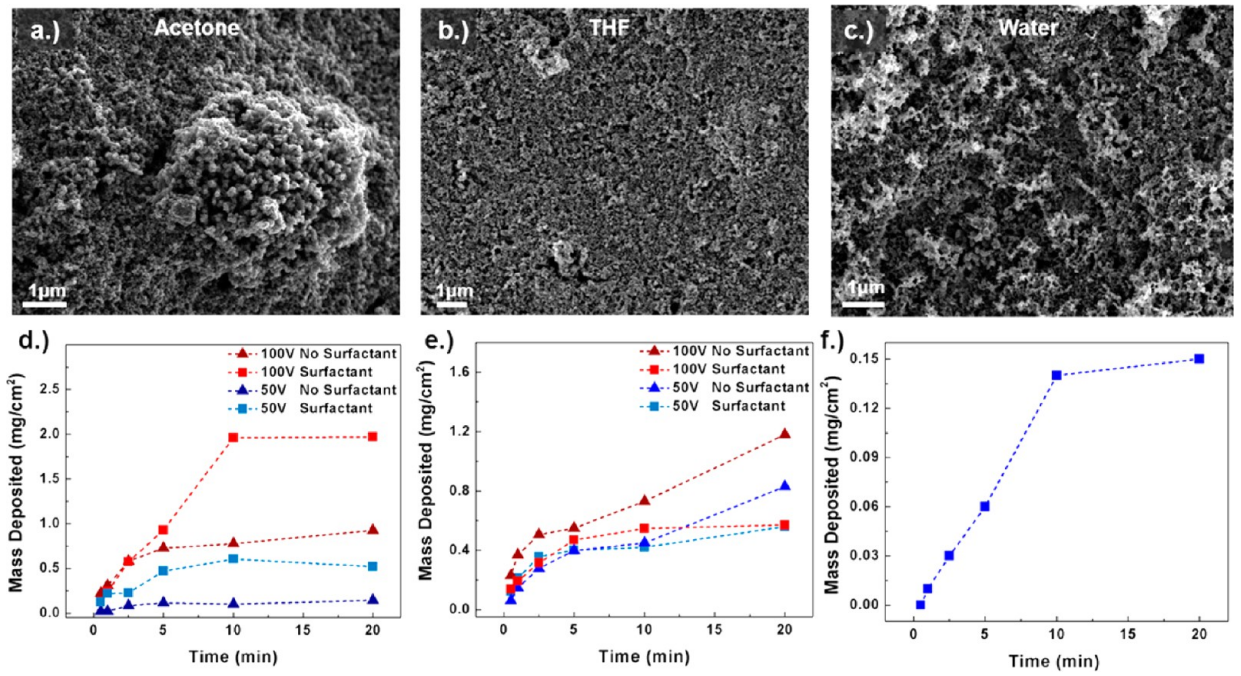


**Figure 2.** (a–c) SEM images showing the CNH film morphology after deposition from (a) acetone, (b) THF, and (c) water. (d–f) Total mass deposited as a function of time for the three solvents shown in a–c, including (d) acetone, (e) THF, and (f) water.

time synthesis scans. Using this approach we are able to produce relatively large amounts of single-walled CNHs with high production rates of 10g/h. CNHs were characterized using scanning and transmission electron microscopy (SEM and TEM), thermogravimetric analysis (TGA), and Raman scattering.[16,36−38]

In our work, single-walled CNHs were synthesized at high temperatures (1150 °C) using high power laser ablation of pure carbon targets and transported to a collector located outside the furnace by atmospheric pressure Ar flow.[16,36−38] Unlike previous studies, which have reported micrometer-size graphitic particles as impurities,[39] our TGA derivative curves showed only one peak at 620 °C corresponding to combustion of CNHs,[16] which is similar to that obtained in previous studies after purification.[39] Additionally, this approach allowed us to eliminate fullerene species by condensing them in a quartz tube zone at the exit of the furnace at temperatures ∼400 °C. Recent efforts employing aberration-corrected, atomic resolution, Z-STEM imaging of single wall CNHs emphasized a small fraction of unconverted graphene flakes on the surface of the CNHs, even though such imaging confirms these surface defects account for much smaller relative surface area compared to that of the CNHs.[37]

**2.2. Electrophoretic Deposition.** Suspensions of CNHs were fabricated by dissolving 10 mg of CNHs into 20 mL of Acetone (Sigma Aldirch, 99.8% Purum), Tetrahydrofuran (Aldrich, 99.8% Purum), and nanopure water (18.6 MΩ resistance). Solutions were shaken vigorously until a homogenous solution was formed. Zeta potential and particle size distribution measurements were performed using a Malvern Zetasizer Nano ZS instrument. Stainless steel electrodes were immersed in the solutions at a separation of 0.3 cm and a voltage of 100 V was applied across the electrodes using an Agilent DC power supply. To achieve deposition on $Al_2O_3$, we evaporated 100 nm $Al_2O_3$ onto conductive silicon wafers using an Angstrom e-beam evaporator. A stainless steel counter electrode was placed 0.3 cm from the silicon electrode and 100 V applied. For deposition on PTFE, 0.1 mm thick PTFE tape was wrapped around the positive stainless steel electrode, separated 0.3 cm from the counter electrode and immersed into the CNH suspension under an applied voltage of 100 V. Deposition on Ni foam was achieved by utilizing 1.6 mm thick, 80 PPI nickel foams (MTI Corp., porosity >95%) directly as the cathode in the electrophoretic cell described previously.

**2.3. Gas Sensing.** Stainless Steel alligator clips were placed onto the active sensing material at a separation of ∼0.2 cm and placed under an applied voltage of 1 V using a Metrohm Autolab sourcemeter in an ambient atmosphere environment. To acquire steady-state conditions, we applied an argon flow at ambient pressure until a steady baseline was achieved. A glass vial of the analyte solutions (Acetone, Aldrich, 99.8% Purum and Toluene, Aldrich, 99.9% Anhydrous) was placed in a separate stainless steel chamber, isolated from the initial argon flow, and given 30 min to achieve repeatable headspace concentrations. To expose the sensor to the analyte vapor, we redirected argon carrier gas through the stainless steel chamber for 5 s before resealing the chamber and exposing the sensor to a pure argon flow (setup shown in Figure S8 in the Supporting Information).

## RESULTS AND DISCUSSION

Upon the synthesis of CNHs, they form spherical aggregates that take on a variety of different morphologies depending on the growth conditions.[40] These aggregates are most often classified as seed, dahlia, bud, and petal-dahlia structures that are formed from curved graphene sheets with edges terminated by short tubules often 2−5 nm in diameter and with cone angles of ∼20°.[40,41] Scanning electron microscope (SEM) and transmission electron microscope (TEM) images of the CNHs utilized in this study emphasize the presence of bud and dahlia-like aggregate structures in accordance with previous studies (Figure 1a−d). This structure leads to the edges of the aggregates and curved carbons to be terminated with reactive $sp^3$ carbons (evident in Raman spectroscopy, see Figure S1a in the Supporting Information), which provides significantly enhanced miscibility in solvents in comparison to other $sp^2$-rich nanocarbons (see Figure S1b in the Supporting Information). This gives EPD a unique advantage as a coating technique to develop CNH-based functional nanomaterials in comparison with other common processing methods.

EPD of CNHs was performed in an electrophoretic cell utilizing two parallel steel electrodes placed approximately 0.3 cm apart in a solution containing CNHs. To achieve

deposition, we applied a voltage across the steel electrodes to generate an electric field that drives the movement of the CNHs toward the charged electrode opposite in sign of the net CNH charge. The mechanism for CNH deposition that explains our observations in this study (Figure 1a) is based on the migration of CNHs toward the cathode due to the net negative charge of the CNH aggregates. Near or at the cathode, the CNH aggregates collide with enough momentum to overpower the aggregate−aggregate Coloumbic repulsion, thereby nucleating clusters of CNHs which then flocculate out from the solution onto the surface. With increasing deposition time, the film continues to grow nonlinearly due to the continuous migration of CNHs toward the solvent-electrode interface that is continuously building up a net repulsive charge. In the framework of this mechanism, the only parameters critical for deposition are the charge/mass ratio of the particles, the electric field at the electrode surface, and the miscibility of the particles in the solvent. The charge/mass ratio of these particles can be estimated by a measurement of the zeta potential in solution (see Figure S2 in the Supporting Information), which is a measurement directly related to the particle mobility in solution. The miscibility of the particles in each solvent is characterized by the hydrodynamic diameter of CNH aggregates obtained using laser Doppler velocimetry (see Figure S3 in the Supporting Information).

To demonstrate the rapid rate at which CNH deposition occurs, Figure 1e−h shows the time evolution of a 0.5 mg/mL initial concentration of CNHs dissolved in acetone subjected to a 4 kV/m electric field applied between two stainless steel plates. In as little as 2 min, visible changes to the optical density of the CNH/acetone solution are observed, and by 6 min, the original highly concentrated, opaque solution of CNHs becomes optically transparent emphasizing the rapid deposition onto the substrate. Analysis of the cathode following deposition (Figure 1j) emphasizes a clean, homogenous, and thick deposition of CNHs that is typical of the coatings studied in this work.

To characterize film formation from different solvents, we investigated deposition of CNHs from suspension of three common solvents including acetone, THF, and nanopure water (Figure 2). Processing from these solvents gives promise to industrial process compatibility, as well as specific materials compatibility (e.g., biocompatible processes). For the deposition from each solvent, we analyzed the rate of mass deposition (in mg/cm$^2$) and morphology of the coating via SEM imaging. We also compare depositions including tetraoctyleammonium-bromate (TOAB) surfactant to depositions that are surfactant free, with the exception of water, where surfactant was required for miscibility. Although we found that we could deposit surfactant-free CNHs from water utilizing oxidized CNHs, our focus in this work is based on the assembly of clean, pristine CNH materials with surface properties only defined by weak mixing treatments in solvents. TOAB is a surfactant with a net negative charge, meaning that it does not compete with the inherent charge of the CNHs. In the case of deposition of CNHs from acetone, we consistently observe a greater deposited mass when a surfactant is utilized, and a greater deposited mass at higher voltages, which is consistent with previous studies.[29,42] However, the greater deposited mass when utilizing the surfactant can be accounted for by consideration of the additional mass deposited because of the presence of the surfactant in the film and conditioning of the electrode surface by surfactant molecules. Evidence for this is supported by measurements of the hydrodynamic particle diameter of the dispersed CNHs with and without surfactant (see Figure S3 in the Supporting Information). In the case when TOAB is utilized as a surfactant, the average particle size increases from 195 to 212 nm, whereas with acetone the average particle size increases from 191 to 199 nm. Although the overall particle mobility with surfactants was measured to be lower (see Figure S2 in the Supporting Information), the improved mass deposition could be due to conditioning of the surface by surfactant molecules that increases the hydrophobicity of the surface and improves the ability for CNHs to adhere to the electrode.[43] In both cases, with and without a surfactant, SEM images emphasized a smooth coating with the presence of some large, apparent nucleation sites (Figure 2a). In general, the overall film morphology was only observed to change slightly between deposition from different solvents, and the presence of TOAB was not found to lead to an alteration of the deposited CNH film features. Comparing the results between acetone and THF solvents, the THF deposited films were smoother and more homogenous with less abundance of large clusters as was observed in the case of deposition from acetone. However, the deposition rate seemed to also be less dependent on the presence of surfactant, and the best deposition rate was measured at 100 V without the presence of surfactant. These results can be further understood by considering the change in zeta potential for dispersions using TOAB as a surfactant versus pristine dispersions. As a greater decrease in the magnitude of the zeta potential indicates lower particle mobility, the measured change in zeta potential (see Figure S2 in the Supporting Information) corresponds well to our experimental observations for mass deposition rates, which are greater in THF ($\zeta$ = −46.4 mV) than acetone ($\zeta$ = −41.1 mV), and greater for surfactant solubilized CNHs in acetone ($\zeta$ = −34.0 mV) than in THF ($\zeta$ = −28.6 mV). Finally, we also studied the deposition of CNHs out of water, which exhibited a lower deposition rate, but a similar trend in the mass deposition as a function of time. The lower deposition rate can be attributed to the smaller applied voltage which was maintained at 1.1 V to avoid electrochemical water reduction/oxidation. SEM images of water-deposited films also show similar film morphology in comparison to the other solvents utilized. In the model for deposition described in Figure 1, we expect this morphology to be caused by the formation of large aggregates representing the competition between van der Waals interactions of adjacent aggregates and CNH aggregate interactions with the solvent that causes flocculation and adhesion to the surface.

To emphasize the versatility of the EPD technique for CNHs, we also deposited onto a variety of different substrates (Figure 3) using CNHs suspended in THF. For stainless steel or conductive substrates, we were able to achieve deposition onto the cathode by using the substrate itself as the electrode. However, for insulating substrates, the insulating layer was suspended near the cathode in a location between the two electrodes to yield deposition (see Figure S4 in the Supporting Information). Although we observe the greatest mass deposition on conductive substrates, we also observe consistent mass deposition profiles for substrates that are not conductive, except with smaller rates of mass deposition. The exponential decay behavior for the film growth as a function of time can be explained by the accumulation of charges on the surface of the substrate where deposition is taking place, causing electrostatic repulsion in the latter stages of film growth. This decay can also

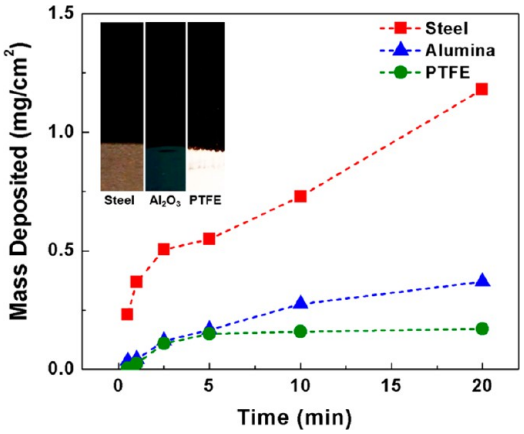


**Figure 3.** Mass deposition as a function of time under identical deposition conditions (100 V, THF, no surfactant), except with different deposition substrates including steel, $Al_2O_3$-coated conductive silicon, and PTFE. Inset are photographs of the black, CNH coatings on the three different substrate materials showing the homogenous nature of the coatings.

be correlated with the measurement of electric current during deposition which, for an EPD process, is representative of the motion and deposition of charged particles in the system. For conductive substrates, we consistently observe an initial rise in the electric current attributed to an increase in CNH concentration near the electrode surface and the corresponding charge transfer upon deposition (see Figure S5 in the Supporting Information). In the case when TOAB surfactant is utilized, the current−time profiles exhibit an exponential decay with time that we ascribe to an initial rapid deposition rate that is inhibited at long times because of the build-up of insulating surfactant layers at the electrode−solvent interface. In contrast to this, the current−time profiles for surfactant-free solutions exhibit a peak in the current followed by a slow decay that we ascribe to the build-up of charge in the CNH coating.

Thick homogenous coatings of CNHs were achieved on all substrates studied, illustrated by photos inset into Figure 3 showing electrodes made of steel, $Al_2O_3$/Si, and PTFE (teflon), which are all coated in optically thick layers of CNHs from acetone-based surfactant-free suspensions. The ability to coat CNHs onto virtually any substrate material represents a capability that is not conventional and particularly novel for EPD of carbon nanomaterials, as only a few studies have shown similar behavior with nanoparticles.[32,33,35] Although we demonstrate this capability here for EPD of CNHs (see Figure S4 in the Supporting Information), we generally observe this technique to be effective for EPD of single-walled CNTs and graphene from similar solvents using TOAB solubilization. Slower deposition rates are consistently observed for insulating substrates compared with conductive substrates, even though

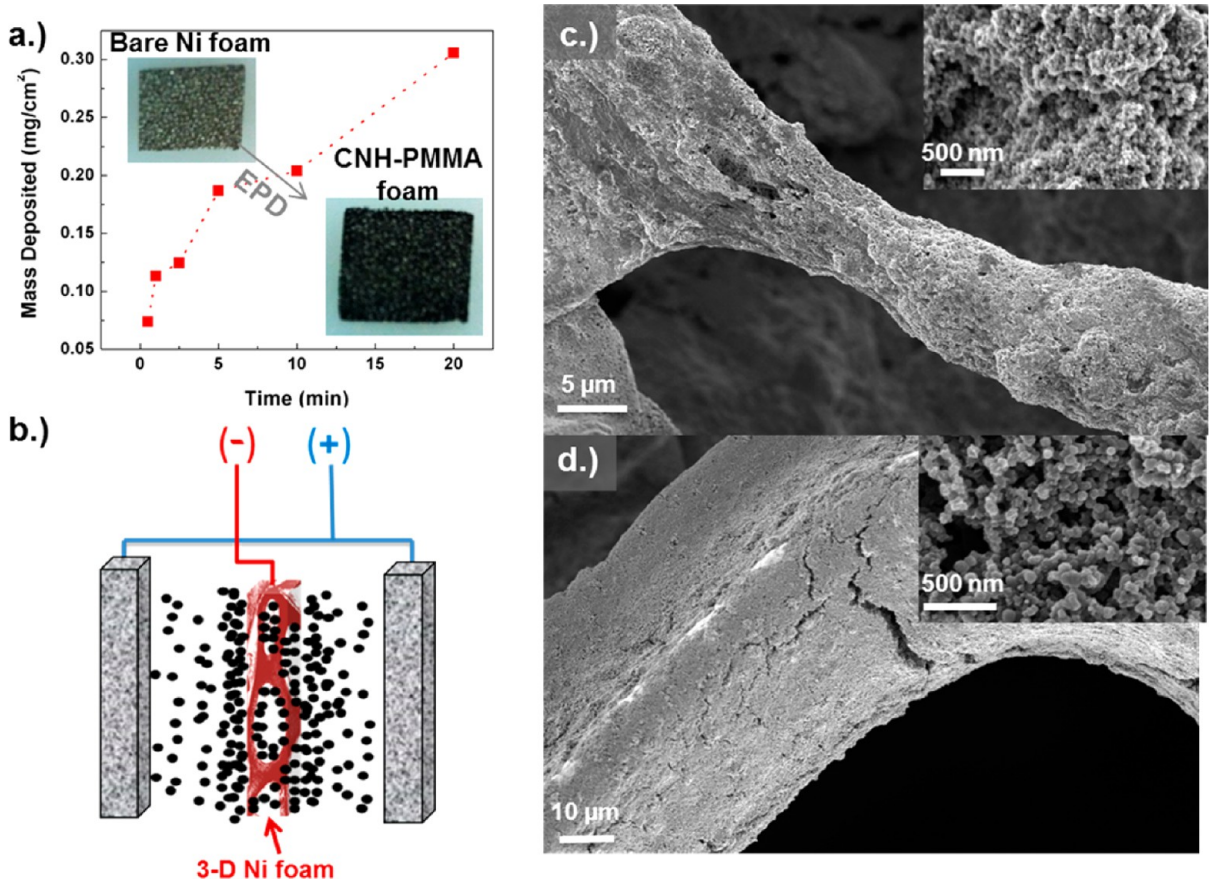


**Figure 4.** (a) CNH mass deposited on a 3D nickel foam as a function of time for depositions performed using acetone as a solvent. Inset is a photograph of a freestanding, 3D CNH-PMMA material that can be achieved after dissolving the Ni foam using HCl. (b) Scheme of the deposition process for 3D substrates, where the cathode is suspended between two conductive electrodes that serve as an anode. (c, d) SEM images of freestanding CNH materials produced by forming PMMA stabilized 3D CNH foams (inset in a), and then dissolving the PMMA support layer. These images emphasize homogenous, 3D coating of CNHs into the foam structure using this technique.

the current-time deposition profiles (see Figure S5 in the Supporting Information) are notably different from conductive substrates and can be correlated to the difference in the dielectric constants of the insulating materials ($\varepsilon_{teflon}$ = 2.1 and $\varepsilon_{alumina}$ = 9.8). This observation provides general insight into the mechanistic process for deposition of these nanomaterials, which is a topic that has remained poorly understood now for decades. Whereas previous studies have suggested mechanisms such as electro-osmotic flows to enable deposition,[28,44] the deposition on an impermeable insulating tape material from solvents where surfactants are not present supports the notion of deposition driven by aggregation and flocculation at the electrode-solvent interface. For single-walled CNTs, which are closely related in structure to the CNHs, the van der Waals interaction energy between two adjacent molecules can be as high as ~0.5 V/m. Therefore, following CNH−CNH collisions near the substrate−solvent interface, the CNHs will tend to aggregate until flocculation occurs due to the instability of the CNH aggregate in solution. This model is supported by the results obtained from depositions from surfactant suspensions versus pristine suspensions of CNHs (see Figure S4 in the Supporting Information), and extends to support our study of insulating substrates as well. We emphasize this as a universal mechanism that can also describe EPD processes for graphene and CNTs as well. As many applications require conductive templates of nanocarbon materials assembled directly on insulating or dielectric surfaces, this approach has significant promise to broaden the potential applications of EPD for nanocarbon materials.

Whereas the most straight-forward EPD substrates are conventionally flat, we demonstrate in this study the promise of using EPD as a technique to form controlled nanocarbon assemblies on three-dimensional (3D) architectures, such as metal foams. This yields the capability to independently control micrometer-scale characteristics of a macroscopically thick material by choice of the 3D material pore size, while controlling the nanoscale features of the material by optimizing parameters of the EPD to yield homogeneity and thickness. Whereas deposition into fabrics or other 3D materials using powders or nanoparticles has been previously achieved,[45−49] we emphasize this route to template uniform films of CNHs into functional 3D macroscopic assemblies. Figure 4 demonstrates the ability to use EPD to coat 3D nickel foam materials with conformal layers of CNHs from acetone or THF solvents. Even though we observe that the CNH coatings penetrate uniformly into the foam materials (see Figure S7 in the Supporting Information), we observe a lower rate of mass increase on the 3D sample. We attribute this to an overall greater surface area at the electrode-solvent interface where the voltage drop is concentrated. This will therefore decrease the strength of the electric field and hence the overall deposition rate, even though the current−time profiles (see Figure S6 in the Supporting Information) indicate the same trend as that observed for EPD onto conductive substrates from pristine surfactant-free solutions of CNHs. Nonetheless, we are able to achieve uniform coatings which may be subsequently suspended in a PMMA matrix. Etching of the Ni foam using a HCl etch solution yields either a PMMA-CNH composite material, or upon dissolving the PMMA, yields a 3D CNH foam material in a manner analogous to 3D graphene materials formed by CVD (Figure 4c, d). However, we note that attempts to stabilize freestanding CNH foam materials without residual polymer led to poor mechanical properties and breaking of the structure. Therefore, although CNH materials independently may not be suited for freestanding, 3D structures, the combination of these materials with other mechanically robust templates can take advantage of the high surface area and edge-site reactivity of the CNHs that can be ideal for catalysis, sensing, field emission,[50] or energy storage and conversion applications.[17,51,52]

Lastly, to emphasize the viability of this one-step approach to making functional assemblies of CNHs on virtually any substrate, comparably deposited CNH and single-walled CNT samples on $Al_2O_3$ were compared for gas sensing applications. Whereas specificity in developing sensing systems is dependent upon ligands or receptors that chemically bind to reactive sites in a material, our focus was to demonstrate the excellent sensitivity that is offered using CNH based materials. We compared optically thick EPD CNH materials to identically prepared single-walled CNTs exhibiting the same total mass in the device because of the well-studied performance of single-walled CNTs as excellent sensing materials,[53,54] and a device configuration that enables comparative behavior between these two materials. For sensing of small exposures of acetone and toluene, which are both trace volatile components in home-made explosive devices,[55,56] we observe the CNHs to exhibit a 2× greater sensitivity with a comparable or slightly reduced response time during conductometric sensing experiments shown in Figure 5 (experimental setup shown in Figure S8 in the Supporting Information). We explain this increased sensitivity due to the requirement for charges to tunnel

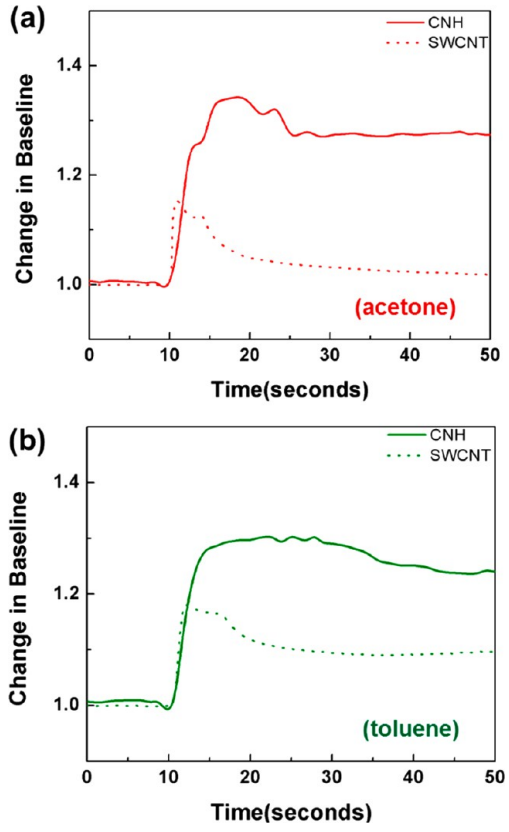


**Figure 5.** Gas detection data from equivalent single-walled CNH and SWCNT films deposited directly on $Al_2O_3$/Si substrates and exposed to (a) acetone and (b) toluene organic species that are common products of homemade IEDs. The analyte was introduced at ~10 s, and CNH films exhibit ~2× better sensitivity, as emphasized by the greater change in conductance baseline in both cases.

between networks of nanometer-scale nanohorns causing the transport behavior and absolute resistance to be highly dependent upon the species that physisorb and interact with the CNH material. This is in comparison to CNTs, which often exist in strands of hundreds of nanometers to a few micrometers, generating fewer CNT−CNT contacts necessary for charges to tunnel across an equally spaced electrode. This is evident from the measured areal conductance measured in the devices of 21.5 and 0.3 mS/cm$^2$ for CNT and CNH devices, respectively, developed to have similar ∼0.38 mg/cm$^2$ mass densities. It should be noted that the basis of our experiments were to demonstrate a technique where one can generate a high sensitivity gas sensor using a one-step approach to fabrication on nonconductive substrates. However, the CNHs also have many sp$^3$ carbon edge sites (unlike single-walled CNTs) that allow them to be functionalized with receptors that can enable specificity, allowing EPD to be a valuable tool for scalable production of CNH sensors deposited on insulating and flexible substrates.

## CONCLUSION

In summary, our results emphasize an inexpensive route toward the development of homogenous coatings of CNHs on virtually any substrate including metals, insulators, and 3D templates using EPD from common solvents including acetone, THF, and water. We propose a flocculation mechanism for the assembly of nanocarbon films that is consistent with our results, and emphasize the promise of EPD as a broadly applicable tool to assembling materials for a wide range of applications, including forming CNH sensing materials with 2× higher sensitivity than comparable single-walled CNTs. As challenges in the development of highly controllable assemblies of nanostructured materials is ultimately a key factor for the future viability of functional templates from many types of nanostructures, such as carbon nanomaterials, this work gives a route to make pristine, rationally designed materials using scalable solution-processed techniques and low-cost solvents. In particular, for single-walled CNHs, the ability to controllably assemble macroscopic materials from these nanostructured building blocks that are developed from bulk growth processes opens new avenues for the development of functional material platforms useful for energy devices, catalysis, sensing, and other applications.

## ASSOCIATED CONTENT

### Supporting Information

(i) Raman spectroscopic analysis of single-walled CNH materials, (ii) zeta potential measurements and details on CNH dispersions in comparison to other sp$^2$-hybridized carbon nanostructures, (iii) current−time profiles for depositions of CNHs on the various substrates studied in this work, (iv) imaging to emphasize the uniformity of coatings in 3D foam materials, (v) electric field distribution models and corresponding electrode geometries for insulating substrates, (vi) a schematic for the setup utilized in gas sensing experiments, and (vii) additional pictures of coatings on stainless steel and PTFE substrates. This material is available free of charge via the Internet at http://pubs.acs.org.

## AUTHOR INFORMATION

### Corresponding Author

*E-mail: cary.l.pint@vanderbilt.edu.

### Notes

The authors declare no competing financial interest.

## ACKNOWLEDGMENTS

This work was supported by Vanderbilt start-up funding and an Oak Ridge Associated Universities Powe Award. CNH synthesis science was sponsored by the Materials Sciences and Engineering (MSE) Division, Office of Basic Energy Sciences, U.S. Department of Energy. Characterization science including Raman spectroscopy, SEM, and TEM part of this research was conducted at the Center for Nanophase Materials Sciences user facility, which is sponsored at Oak Ridge National Laboratory by the Scientific User Facilities (SUF) Division, U.S. Department of Energy.

## REFERENCES

(1) Chen, Y.; Zhang, X.; Yu, P.; Ma, Y. W. *J. Power Sources* **2010**, *195* (9), 3031−3035.
(2) Chen, Z. P.; Ren, W. C.; Gao, L. B.; Liu, B. L.; Pei, S. F.; Cheng, H. M. *Nat Mater* **2011**, *10* (6), 424−428.
(3) Dong, X. C.; Ma, Y. W.; Zhu, G. Y.; Huang, Y. X.; Wang, J.; Chan-Park, M. B.; Wang, L. H.; Huang, W.; Chen, P. *J. Mater. Chem.* **2012**, *22* (33), 17044−17048.
(4) Yavari, F.; Chen, Z. P.; Thomas, A. V.; Ren, W. C.; Cheng, H. M.; Koratkar, N. *Sci. Rep.* **2011**, *1*, 166.
(5) De Volder, M.; Tawfick, S. H.; Park, S. J.; Copic, D.; Zhao, Z. Z.; Lu, W.; Hart, A. J. *Adv. Mater.* **2010**, *22* (39), 4384.
(6) Behabtu, N.; Green, M. J.; Pasquali, M. *Nano Today* **2008**, *3* (5-6), 24−34.
(7) Behabtu, N.; Lomeda, J. R.; Green, M. J.; Higginbotham, A. L.; Sinitskii, A.; Kosynkin, D. V.; Tsentalovich, D.; Parra-Vasquez, A. N. G.; Schmidt, J.; Kesselman, E.; Cohen, Y.; Talmon, Y.; Tour, J. M.; Pasquali, M. *Nat. Nanotechnol.* **2010**, *5* (6), 406−411.
(8) Behabtu, N.; Young, C. C.; Tsentalovich, D. E.; Kleinerman, O.; Wang, X.; Ma, A. W. K.; Bengio, E. A.; ter Waarbeek, R. F.; de Jong, J. J.; Hoogerwerf, R. E.; Fairchild, S. B.; Ferguson, J. B.; Maruyama, B.; Kono, J.; Talmon, Y.; Cohen, Y.; Otto, M. J.; Pasquali, M. *Science* **2013**, *339* (6116), 182−186.
(9) Ma, A. W. K.; Nam, J.; Behabtu, N.; Mirri, F.; Young, C. C.; Dan, B.; Tsentalovich, D.; Majumder, M.; Song, L.; Cohen, Y.; Ajayan, P. M.; Pasquali, M. *Ind. Eng. Chem. Res.* **2013**, *52* (26), 8705−8713.
(10) Parra-Vasquez, A. N. G.; Behabtu, N.; Green, M. J.; Pint, C. L.; Young, C. C.; Schmidt, J.; Kesselman, E.; Goyal, A.; Ajayan, P. M.; Cohen, Y.; Talmon, Y.; Hauge, R. H.; Pasquali, M. *Acs Nano* **2010**, *4* (7), 3969−3978.
(11) Bergin, S. D.; Nicolosi, V.; Streich, P. V.; Giordani, S.; Sun, Z. Y.; Windle, A. H.; Ryan, P.; Niraj, N. P. P.; Wang, Z. T. T.; Carpenter, L.; Blau, W. J.; Boland, J. J.; Hamilton, J. P.; Coleman, J. N. *Adv. Mater.* **2008**, *20* (10), 1876.
(12) Bergin, S. D.; Sun, Z. Y.; Streich, P.; Hamilton, J.; Coleman, J. N. *J. Phys. Chem. C* **2010**, *114* (1), 231−237.
(13) Majumder, M.; Rendall, C. S.; Eukel, J. A.; Wang, J. Y. L.; Behabtu, N.; Pint, C. L.; Liu, T. Y.; Orbaek, A. W.; Mirri, F.; Nam, J.; Barron, A. R.; Hauge, R. H.; Schmid, H. K.; Pasquali, M. *J. Phys. Chem. B* **2012**, *116* (22), 6536−6542.
(14) Zhu, S. Y.; Xu, G. B. *Nanoscale* **2010**, *2* (12), 2538−2549.
(15) Pagona, G.; Mountrichas, G.; Rotas, G.; Karousis, N.; Pispas, S.; Tagmatarchis, N. *Int. J. Nanotechnol.* **2009**, *6* (1-2), 176−195.
(16) Cheng, M. D.; Lee, D. W.; Zhao, B.; Hu, H.; Styers-Barnett, D. J.; Puretzky, A. A.; DePaoli, D. W.; Geohegan, D. B.; Ford, E. A.; Angelini, P. *Nanotechnology* **2007**, *18* (18), 185604.
(17) Izadi-Najafabadi, A.; Yamada, T.; Futaba, D. N.; Yudasaka, M.; Takagi, H.; Hatori, H.; Iijima, S.; Hata, K. *ACS Nano* **2011**, *5* (2), 811−819.
(18) Zhao, Y.; Li, J. X.; Ding, Y. H.; Guan, L. H. *Chem. Commun.* **2011**, *47* (26), 7416−7418.

(19) Yoshitake, T.; Shimakawa, Y.; Kuroshima, S.; Kimura, H.; Ichihashi, T.; Kubo, Y.; Kasuya, D.; Takahashi, K.; Kokai, F.; Yudasaka, M.; Iijima, S. *Physica B* **2002**, *323* (1-4), 124−126.
(20) Kasuya, D.; Yudasaka, M.; Takahashi, K.; Kokai, F.; Iijima, S. *J. Phys. Chem. B* **2002**, *106* (19), 4947−4951.
(21) Yuge, R.; Yudasaka, M.; Toyama, K.; Yamaguchi, T.; Iijima, S.; Manako, T. *Carbon* **2012**, *50* (5), 1925−1933.
(22) Azami, T.; Kasuya, D.; Yuge, R.; Yudasaka, M.; Iijima, S.; Yoshitake, T.; Kubo, Y. *J. Phys. Chem. C* **2008**, *112* (5), 1330−1334.
(23) Biswas, J.; Rottman-Yang, J. S.; Gonzalo-JuanA, I.; Dickerson, J. H. *J. Electrochem. Soc.* **2012**, *159* (4), K103−K106.
(24) Chavez-Valdez, A.; Shaffer, M. S. P.; Boccaccini, A. R. *J. Phys. Chem. B* **2013**, *117* (6), 1502−1515.
(25) Hasan, S. A.; Rigueur, J. L.; Harl, R. R.; Krejci, A. J.; Gonzalo-Juan, I.; Rogers, B. R.; Dickerson, J. H. *ACS Nano* **2010**, *4* (12), 7367−7372.
(26) Mazurenko, I.; Etienne, M.; Tananaiko, O.; Urbanova, V.; Zaitsev, V.; Walcarius, A. *Carbon* **2013**, *53*, 302−312.
(27) Corni, I.; Ryan, M. P.; Boccaccini, A. R. *J. Eur. Ceram. Soc.* **2008**, *28* (7), 1353−1367.
(28) Sarkar, P.; Nicholson, P. S. *J. Am. Ceram. Soc.* **1996**, *79* (8), 1987−2002.
(29) Kamat, P. V.; Thomas, K. G.; Barazzouk, S.; Girishkumar, G.; Vinodgopal, K.; Meisel, D. *J. Am. Chem. Soc.* **2004**, *126* (34), 10757−10762.
(30) Davis, V. A.; Parra-Vasquez, A. N. G.; Green, M. J.; Rai, P. K.; Behabtu, N.; Prieto, V.; Booker, R. D.; Schmidt, J.; Kesselman, E.; Zhou, W.; Fan, H.; Adams, W. W.; Hauge, R. H.; Fischer, J. E.; Cohen, Y.; Talmon, Y.; Smalley, R. E.; Pasquali, M. *Nat. Nanotechnol.* **2009**, *4* (12), 830−834.
(31) Hernandez, Y.; Nicolosi, V.; Lotya, M.; Blighe, F. M.; Sun, Z. Y.; De, S.; McGovern, I. T.; Holland, B.; Byrne, M.; Gun'ko, Y. K.; Boland, J. J.; Niraj, P.; Duesberg, G.; Krishnamurthy, S.; Goodhue, R.; Hutchison, J.; Scardaci, V.; Ferrari, A. C.; Coleman, J. N. *Nat. Nanotechnol.* **2008**, *3* (9), 563−568.
(32) Hasan, S. A.; Kavich, D. W.; Dickerson, J. H. *Chem. Commun.* **2009**, *25*, 3723−3725.
(33) Hasan, S. A.; Kavich, D. W.; Mahajan, S. V.; Dickerson, J. H. *Thin Solid Films* **2009**, *517* (8), 2665−2669.
(34) Leone, A.; Marino, W.; Scharifker, B. R. *J. Electrochem. Soc.* **1992**, *139* (2), 438−443.
(35) Tada, K. *IEICE Trans. Electron* **2013**, *E86c* (3), 378−380.
(36) Chandrakumar, K. R. S.; Readle, J. D.; Rouleau, C.; Puretzky, A.; Geohegan, D. B.; More, K.; Krishnan, V.; Tian, M. K.; Duscher, G.; Sumpter, B.; Irle, S.; Morokuma, K. *Nanoscale* **2013**, *5* (5), 1849−1857.
(37) Liu, Y.; Brown, C. M.; Neumann, D. A.; Geohegan, D. B.; Puretzky, A. A.; Rouleau, C. M.; Hu, H.; Styers-Barnett, D.; Krasnov, P. O.; Yakobson, B. I. *Carbon* **2012**, *50* (13), 4953−4964.
(38) Puretzky, A. A.; Styers-Barnett, D. J.; Rouleau, C. M.; Hu, H.; Zhao, B.; Ivanov, I. N.; Geohegan, D. B. *Appl. Phys. A* **2008**, *93* (4), 849−855.
(39) Zhang, M.; Yudasaka, M.; Miyawaki, J.; Fan, J.; Iijima, S. *J. Phys. Chem. B* **2005**, *109* (47), 22201−22204.
(40) Bandow, S.; Kokai, F.; Takahashi, K.; Yudasaka, M.; Qin, L. C.; Iijima, S. *Chem. Phys. Lett.* **2000**, *321* (5-6), 514−519.
(41) Xu, J. X.; Tomimoto, H.; Nakayama, T. *Carbon* **2011**, *49* (6), 2074−2078.
(42) Boccaccini, A. R.; Cho, J.; Roether, J. A.; Thomas, B. J. C.; Minay, E. J.; Shaffer, M. S. P. *Carbon* **2006**, *44* (15), 3149−3160.
(43) Pignolet, C.; Filiatre, C.; Foissy, A. *Langmuir* **2008**, *24* (18), 10181−10186.
(44) Bohmer, M. *Langmuir* **1996**, *12* (24), 5747−5750.
(45) Boccaccini, A. R.; Trusty, P. A. *J. Mater. Sci.* **1998**, *33* (4), 933−938.
(46) Coupe, A.; Maskrot, H.; Buet, E.; Renault, A.; Fontaine, P. J.; Chaffron, L. *J. Eur. Ceram. Soc.* **2012**, *32* (14), 3837−3850.
(47) Heim, M.; Reculusa, S.; Ravaine, S.; Kuhn, A. *Adv. Funct. Mater.* **2012**, *22* (3), 538−545.
(48) Moritz, K.; Muller, E. *Key Eng. Mater.* **2002**, *206-2*, 193−196.
(49) Palmer, T. R.; Buie, C. R. Fundamentals of Pulsed and Direct Current Electrophoretic Infiltration Kinetics. In *Electrophoretic Deposition: Fundamentals and Applications IV*; Boccaccini, A. R., Van der Biest, O., Clasen, R., Dickerson, J. H., Eds.; Trans Tech Publications: Dürnten, Switzerland, 2012; pp 53−60.
(50) Yuge, R.; Miyawaki, J.; Ichihashi, T.; Kuroshima, S.; Yoshitake, T.; Ohkawa, T.; Aoki, Y.; Iijima, S.; Yudasaka, M. *Acs Nano* **2010**, *4* (12), 7337−7343.
(51) Sani, E.; Mercatelli, L.; Barison, S.; Pagura, C.; Agresti, F.; Colla, L.; Sansoni, P. *Sol. Energy Mater. Sol. Cells* **2011**, *95* (11), 2994−3000.
(52) Yuge, R.; Manako, T.; Nakahara, K.; Yasui, M.; Iwasa, S.; Yoshitake, T. *Carbon* **2012**, *50* (15), 5569−5573.
(53) Li, J.; Lu, Y. J.; Ye, Q.; Cinke, M.; Han, J.; Meyyappan, M. *Nano Lett.* **2003**, *3* (7), 929−933.
(54) Robinson, J. A.; Snow, E. S.; Badescu, S. C.; Reinecke, T. L.; Perkins, F. K. *Nano Lett.* **2006**, *6* (8), 1747−1751.
(55) Dobrokhotov, V.; Oakes, L.; Sowell, D.; Larin, A.; Hall, J.; Kengne, A.; Bakharev, P.; Corti, G.; Cantrell, T.; Prakash, T.; Williams, J.; McIlroy, D. N. *J. Appl. Phys.* **2012**, *111* (4), 044311.
(56) Armitt, D.; Zimmermann, P.; Ellis-Steinborner, S. *Rapid Commun. Mass Spectrom.* **2008**, *22* (7), 950−958.